Available online at www.sciencedirect.com
ScienceDirect
Journal of Power Sources 171 (2007) 8–17
JOURNAL OF POWER SOURCES
www.elsevier.com/locate/jpowsour

Performance of thin-film cathodes for proton-exchange-membrane fuel cells based on high-surface-area carbon supports

G.J.M. Janssen *, E.F. Sitters

Energy Research Centre of the Netherlands ECN, P.O. Box 1, 1755 ZG Petten, The Netherlands

Received 15 September 2006; received in revised form 1 November 2006; accepted 6 November 2006
Available online 8 December 2006

Abstract

New commercial catalysts materials from Johnson Matthey were tested in thin-film electrodes (cathodes) in PEMFCs. These catalysts are nano-sized Pt particles on a novel high-surface-area carbon support. It was found that in thin-film electrodes made from the new catalyst material a much higher specific electrochemically active surface area could be achieved than in electrodes made from conventional 40 wt% Pt/Vulcan XC-72. This was due to both smaller particle sizes and a better utilisation, and also resulted in a higher mass activity. The optimum Nafion content was found to be 20 wt%. The thickness of electrodes was reduced, resulting in a lower proton resistance. This reduced the transport losses in the electrode, as is also illustrated by modelling results.

Keywords: Proton exchange membrane fuel cell; Cathode active layer; Electrochemical impedance spectroscopy; Transport properties; Electrode models

1. Introduction

Both for reasons of cost and of availability of Pt, the reduction of the required amount of Pt has always been the main focus of PEMFC electrode research and development. State-of-the-art electrodes have a Pt loading in the order of 0.4 mg cm^{-2} [1,2]. Inspection of data provided by commercial manufacturers [3–7] and in the literature [1,2] shows that at operating temperatures of 65–80 °C a power density in the order 0.5–0.6 W cm^{-2} at 0.65 V can be achieved and possibly up to 0.7 W cm^{-2}.

However, for automotive applications a further reduction of the Pt loading is needed. Gasteiger et al. [1] indicated that the target for hydrogen/air fuel cells in automotive applications should be a total Pt loading of the membrane-electrode-assembly (MEA) of 0.15 mg Pt cm^{-2}. The required performance should be 0.8–0.9 W cm^{-2} at cell voltages of 0.65 V or higher. This translates to 0.2 g Pt kW^{-1} or 16 g Pt for a vehicle equipped with an 80 kW system. For the anode it seems that the Pt loading can be reduced from 0.4 to 0.05 mg cm^{-2} with very small additional voltage losses [8]. Reduction of the cathode Pt loading to 0.1 mg cm^{-2} while at the same time increasing the performance from 0.5 to 0.8 W cm^{-2} remains a challenge. In state-of-the-art cathodes voltage losses are in the order of 400 mV. The majority hereof is due to the sluggish kinetics of the oxygen reduction reaction, but also to limited proton conduction and, especially at high current density, limited oxygen transport. Moreover, the fraction of Pt surface area that is electrochemically active, i.e. connected to the carbon backbone as well as to the proton conducting ionomer phase, is limited. Optimisation of the structure seems essential to reduce the cathode losses.

State-of-the-art cathodes are so-called thin film electrodes that consist of catalysed carbon black supporting nano-sized Pt particles, and ionomer (Nafion). The microstructure of thin film electrodes is quite complex [9,10]. It consists of carbon agglomerates with both the intra-agglomerate as well as the inter-agglomerate pores to some extent filled with ionomer. Up to now the preferred carbon support was Vulcan XC-72. This carbon black has a specific surface area of 220–250 m^2 g^{-1} which is sufficiently high for the deposition of 20–40 wt% of Pt nanoparticles, achieving a specific surface area for platinum in the order of 70–120 m^2 g^{-1} [3,11]. A higher specific surface area of the carbon black would allow a higher Pt loading on the carbon, which would result in thinner electrodes as the amount of carbon required is reduced. However, in the past it was found that on high-surface-area carbon supports a large fraction of the Pt particles was in small pores inaccessible to Nafion

* Corresponding author. Tel.: +31 224 56 4803; fax: +31 224 56 8489.
E-mail address: janssen@ecn.nl (G.J.M. Janssen).

0378-7753/$ – see front matter © 2006 Elsevier B.V. All rights reserved.
doi:10.1016/j.jpowsour.2006.11.008

Nomenclature

a	distance between Pt particle on a support (cm)
b	Tafel slope of the oxygen reduction electro reaction (V or mV dec^{-1})
C_{dl}	double layer capacitance of the electrode ($F\,cm^{-2}$)
d	Pt particle size (cm)
E^0	thermodynamic open circuit potential (V)
ECSA	electrochemically active surface area ($m^2\,g^{-1}$ Pt)
F	Faraday constant (96,485 $C\,mol^{-1}$)
i_m	mass activity of the platinum ($A\,g^{-1}$)
i_s	specific activity of the platinum ($A\,cm^{-2}$ Pt)
i_x	current density equivalent to the hydrogen cross-over ($A\,cm^{-2}$)
i_0	exchange current density parameter ($A\,cm^{-2}$)
j	current density in the cell ($A\,cm^{-2}$)
j_{crit}, j_{dif}	critical current density for proton transport and oxygen diffusion limitations, respectively ($A\,cm^{-2}$)
j_H	proton current density ($A\,cm^{-2}$)
L	thickness of the electrode (cm)
m_{Pt}	platinum content of the electrode ($mg\,cm^{-2}$)
pH_2, pO_2	hydrogen/oxygen partial pressure at the anode/cathode (bar)
P_m	oxygen permeability ($mol\,s^{-1}\,cm^{-1}\,bar^{-1}$)
R	gas constant ($8.31\,J\,mol^{-1}\,K^{-1}$)
R_{hf}	ohmic resistance of the cell ($\Omega\,cm^2$)
R_p	proton resistance in electrode ($\Omega\,cm^2$)
SA	specific surface area ($m^2\,g^{-1}$)
T	cell temperature (K)
u	utilisation of Pt, ratio of ECSA and SA of Pt
V_{cell}	cell voltage (V)
$V_{IR\text{-}corr}$	cell voltage corrected for ohmic losses (V)
w	Pt weight fraction catalyst powder
X	characteristic diffusion parameter in the agglomerate model ($A\,cm^{-2}$)
y	oxygen pressure at the cathode relative to a reference pressure
Z_t^{hf}	total (complex) impedance at high frequencies ($\Omega\,cm^2$)

Greek letters

ε	volume fraction
$\eta(z)$, η_1	local and total cathode overpotential:potential difference between the electron conducting phase and the proton conducting phase in the cathode relative to the to the standard difference (V)
ρ_{Pt}	density of platinum ($g\,cm^{-3}$)
σ_{ion}	proton conductivity of the ionomer phase ($S\,cm^{-1}$)
ω	angular frequency (s^{-1})

[12,13]. Recently, Tanaka Kikinzoku International K.K. (TKK) and Johnson Matthey (JM) have brought Pt catalysts on the market with novel high-surface-area supports that they claim would be better suited for fuel cell applications [6,11].

The performance of the electrode also depends strongly on the Nafion content. For electrodes based upon 20–40 wt% Pt/Vulcan XC-72 the optimum Nafion content is well documented and in the order of 30 wt% [14–17]. The use of the novel supports requires a re-optimisation of the Nafion:carbon ratio. In this paper the application of the Johnson Matthey Hispec® 9100 catalysts, i.e. 56 wt% Pt on the novel AC01 support, in thin-film electrodes is investigated. For varying Nafion content, the utilisation, kinetics, proton transport and gas transport were studied by means of structural and electrochemical characterisation. Electrode models were used to interpret the results.

2. Experimental

2.1. Structural characterisation

The as-received catalysts powders were characterised by nitrogen physisorption at 77 K using a Coulter Omnisorp360. Structural characterisation of the membrane-electrode-assemblies (MEAs) was carried out with a JEOL 6330F scanning electron microscope.

2.2. Manufacturing of MEAs

An ink was made consisting of Pt/carbon Hispec® 9100 material (56 wt% Pt on high-surface-area carbon, purchased from AlfaAesar) dissolved in 1,2-propanediol to which a Nafion® solution (25 wt% in 1,2 propanediol) was added. The Nafion content was varied to end up with 10, 15, 20, 30 and 40 wt% Nafion in the dry electrode material. An additive was used to stabilize the solution. This ink was subsequently screen-printed on a gas diffusion medium (GDM) i.e. Sigracet® GDL 31BC from SGL Carbon. The targeted Pt loading was 0.4 $mg\,cm^{-2}$. The material was dried and Pt loadings were determined by weighing. On these electrodes a solution of 10% Nafion in water/3% butanol was applied, with a target Nafion loading of 0.05 $mg\,cm^{-2}$. After another drying step, a N112 membrane from Dupont was sandwiched between two electrodes. The MEA was pressed at 130 °C during 90 s at 40 bar. The active geometric surface area of the MEAs was 7 cm^2.

Following the same recipe, MEAs were made from 40 wt% Pt/Vulcan XC-72 from E-TEK, but only with 30 wt% Nafion in the dry electrode material.

2.3. Electrochemical testing of MEAs

The MEAs were mounted in a fuel cell test rig. They were clamped between two graphite plates in which a serpentine channel had been machined. The cells were tested with hydrogen (stoichiometric ratio 1.5) at the anode and oxygen or air (stoichiometric ratio 2) at the cathode. Atmospheric pressure was used at both sides. The cell temperature was 65 °C, and the gases

were humidified at cell temperature. *V–j* characteristics were recorded using an electronic load. At several current densities electrochemical impedance spectroscopy (EIS) measurements were done using a Zahner IM6e with a PP200 power potentiostat, with frequency between 100 kHz and 1 Hz. In these cases oxygen was fed to the cathode. The anode operating under hydrogen was used as reference and counter electrode.

In addition *in situ* cyclic voltammograms were taken from the cathode. To this end nitrogen was flushed at the cathode side, which was the working electrode in these experiments and hydrogen at the anode side, which was used as the counter and reference electrode, and the measurements were carried out at 25 °C. For these measurements an EG&G 273A potentiostat/galvanostat was used.

3. Results

3.1. Characterisation of the catalyst

According to the supplier, the E-TEK material had a specific Pt surface area (SA) of 72 $m^2\ g^{-1}$ with an average particle size of 3.9 nm. For the Hispec 9100 material these values are 105 $m^2\ g^{-1}$ and 2.5 nm, respectively. The specific surface area (BET) for Vulcan is 250 $m^2\ g^{-1}$. The measured total BET surface area of the Hispec 9100 powder was 318 $m^2\ g^{-1}$, and of the E-TEK powder 134 $m^2\ g^{-1}$. A value for the AC01 specific surface area was not given by the supplier, but from comparison of the data on the BET surface area of the catalysts, the Pt fractions and the SA of Pt in the respective powders, the specific surface area of AC01 was estimated to be 700–800 $m^2\ g^{-1}$.

The N_2 adsorption isotherms were recalculated to the amount of carbon is the samples, assuming that Pt did not contribute to the porosity. They are shown in Fig. 1a. The isotherms show enhanced micro- and mesoporosity of the AC01 support of the Hispec9100 material compared to Vulcan XC-72 support of the E-TEK catalyst. The pore size distribution in Fig. 1b, calculated from the desorption branch of the isotherm using the Barrett–Joyner–Halenda model, confirms the large mesopore volume, and a slight shift to somewhat larger pore sizes in AC01 compared to Vulcan. The pore volume of pores with size between 4 and 67 nm was 0.32 ml g_C^{-1} for Hispec 9100 and 0.17 ml g_C^{-1} for the E-TEK catalyst.

According to Uchida [12], a minimum distance between Pt particles is required to prevent them from coagulation. This means that on carbon supports with a higher specific surface area more particles can be loaded per unit carbon weight. Assuming a closest packing geometry on the surface, each Pt particle has associated with it a carbon surface area of $1/2\sqrt{3}a^2$, with a the distance between Pt particles. For Pt particles with size d, and a weight fraction w on a support with a specific surface area SA_C the distance a is given by

$$a = \frac{1}{3}\sqrt{\frac{\sqrt{3}\pi\rho_{Pt}d^3SA_C(1-w)}{w}} \quad (1)$$

Identifying SA_C with the BET surface area of carbon, Uchida [12] obtained values in the order of 10 nm for several carbon black supports. With the data for Hispec 9100 catalysts the result was $a \approx 11$ nm, and for E-TEK 40 wt% Pt/Vulcan XC-72 $a \approx 10$ nm, in good agreement with results by Uchida. Increasing the Pt weight fraction on Vulcan to order 56 wt% results in an increased particle size and further reduced SA of Pt [3,11,18].

3.2. Structural characterisation of the electrode

The thickness of electrodes was determined from SEM micrographs, an example of which is shown in Fig. 2a. Electrodes containing ≥20 wt% Nafion are visible as thin uniform layers with a good contrast with the membrane and GDM. The thickness of these layers based on Hispec 9100 is in the order of 8 μm, compared to 11 μm for the layer made from E-TEK material. In the case of low Nafion content it was more difficult to establish a layer thickness as the layer was not very homogeneous. Still, the average layer thickness seemed comparable to those of electrodes with more Nafion.

The reduction in thickness of AC01 based electrodes versus the Vulcan XC-72 based electrode was smaller than the reduction of the amount of carbon in the layers, which was almost 50%. Table 1 lists the volume composition of the layers. The volume fractions were calculated from the composition and thickness

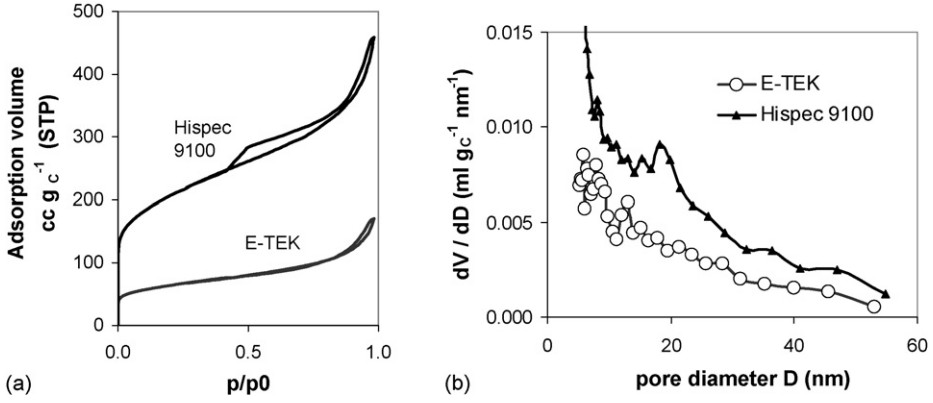

Fig. 1. (a) N_2 adsorption isotherm and (b) calculated pore size distribution of Hispec 9100 and E-TEK catalyst materials. The adsorbed volumes are normalised to the amount of carbon in both samples.

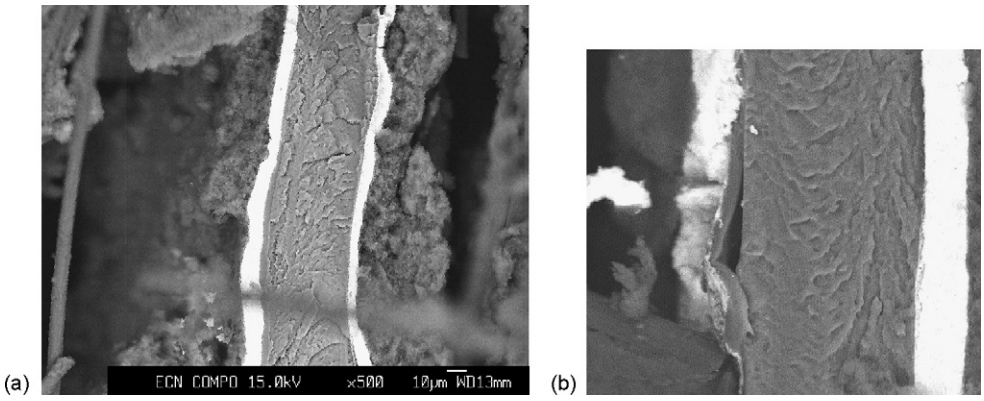

Fig. 2. (a) SEM micrograph of the cross-section of MEAs with electrodes containing Hispec 9100 and 40 wt% Nafion. The bright sections on each side of the membrane are the electrodes. (b) Magnification of a SEM micrograph showing the interfacial Nafion layer between the electrode and the membrane.

of the layer and the density of the components, i.e. 2 g cm^{-3} for carbon, 2 g cm^{-3} for Nafion and 21.5 g cm^{-3} for Pt. The volume occupied by the AC01 carbon structure is in the order of 20 vol%, whereas the Vulcan XC-72 occupies 27 vol% of the layer. Compared to the Vulcan XC-72 structure in the electrode, the AC01 structure upon is more porous, in agreement with the N_2 physisorption data reported above. With increasing Nafion content the fraction of voids decreases in the Hispec 9100 electrodes, as more voids in the carbon skeleton are filled with Nafion. This is in agreement with results for Vulcan based electrodes by Gode et al. [19].

Further inspection of the SEM micrographs, as shown in Fig. 2b, showed that the additional Nafion layer was indeed present in the form of a thin layer, i.e. the Nafion did not deeply penetrate the active layer.

3.3. Cyclic voltammetry

Cyclic voltammetry was used to determine the electrochemically active surface area (ECSA) and the double layer capacitance of the cathode as a function of the wt% Nafion (Table 2). The ECSA was calculated assuming 210 μC cm^{-2} Pt. The relation between the ECSA and SA is given by the metal utilisation u [13,20]

$$\text{ECSA} = \text{SA} \times u \quad (2)$$

The data in Table 2 show that the electrodes prepared from the catalysts supported on the new high-surface-area carbon have a higher ECSA than the ones based upon 40 wt% Pt/Vulcan catalysts. The results obtained with the Vulcan based electrodes compare well to data in the literature [1]. The high ECSA of the Hispec 9100 electrodes is due to the higher SA of Pt and to a better utilisation. Utilisation is less than 100% due to either poor coverage of Pt by Nafion or to encapsulation of the carbon by Nafion, which disconnects the Pt particle from the electron conducting network. At 20 wt% Nafion the utilisation showed a slight maximum.

The double layer capacitance was also obtained from the cyclic voltammetry data. The electrical capacitance is a measure of the surface area, both of Pt and C that can be accessed by electrons as well as protons. The values in the order of 53 F g^{-1} obtained for the AC01 based electrodes are significantly higher than for the Vulcan based electrode. The value of 30 F g^{-1} for the 40 wt% Pt/Vulcan electrode agrees well with the value of 37 F g^{-1} catalyst (20 wt% Pt on Vulcan) reported by Easton and Pickup [21]. The increased capacitance of the AC01 based electrodes reflects the higher specific surface area of the carbon and Pt. With exception of the electrode with 10 wt% of Nafion, the capacitance was nearly independent of the Nafion content.

3.4. Kinetic activity

The kinetic activity of the electrodes was estimated from the low current density part of the V–j curves measured with oxygen. To this end the curves were corrected for the ohmic losses R_{hf} and the hydrogen cross-over through the membrane, equivalent to a current density i_x [8]. The anode losses were neglected. The

Table 1
Structural parameters of electrodes with 0.4 mg cm^{-2} Pt loading

	Hispec 9100 56 wt% Pt AC01					E-TEK 40 wt% Pt Vulcan XC-72
Nafion wt%	10	15	20	30	40	30
Thickness (μm)	8	8	8	8	8	11
ε (void) (%)	74	70	64	59	47	54
ε (carbon) (%)	19	20	21	20	20	27
ε (Nafion) (%)	5	8	12	19	30	17
Ionomer:carbon volume ratio	0.3	0.4	0.6	1.0	1.5	0.6

Table 2
ECSA and utilisation of electrodes

	Hispec 9100 56 wt% Pt AC01					E-TEK 40 wt% Pt Vulcan XC-72
SA_{Pt} $m^2\,g^{-1}$ (CO-ads)	105	105	105	105	105	72
Nafion wt%	10	15	20	30	40	30
ECSA MEA $m^2\,g^{-1}$ Pt	62	64	67	60	63	33
Utilisation	59	61	64	57	60	41
Double layer capacitance ($F\,g^{-1}$)	72	53	53	46	53	30

IR-corrected *V–j* curve was calculated according to

$$V_{\text{IR-corr}}(j + i_x) = V_{\text{cell}}(j) + j \times R_{\text{hf}} \quad (3)$$

Values for R_{hf} were obtained by EIS as the high frequency intercept at the real axis in the Nyquist plots. Since the values were similar with an average of $0.078\,\Omega\,\text{cm}^2$ for all MEAs it was decided to use this value for all curves. A similar value for all MEAs was expected, since apart from the Nafion content in the electrode all components were the same. The electrode electronic resistance is negligible, as long as a percolating carbon network exists. The use of a single value for R_{hf} implies that all differences between curves were directly related to differences in cathode losses.

Following the method in ref. [2], a value of $1\,\text{mA}\,\text{cm}^{-2}$ for i_x was obtained for N112 membranes at the present operating conditions, in agreement with measurements for N112 membranes elsewhere [1,2]. The IR-corrected *V–j* curves obtained with, respectively, 10, 20 and 40 wt% Nafion content in the electrodes are shown Fig. 3 as Tafel plots.

Commonly used measures for the kinetic activity of the cathode are the mass activity i_{m} and specific activity i_{s} at 0.9 V, IR-corrected [1,22]. For a cathode with Pt loading m_{Pt} these quantities are defined by

$$i_{\text{m}}\,\text{at}\,0.9\,V_{\text{IR-corr}} = \frac{j\,\text{at}\,V_{\text{IR-corr}} = 0.9\,\text{V}}{m_{\text{Pt}}} \quad (4)$$

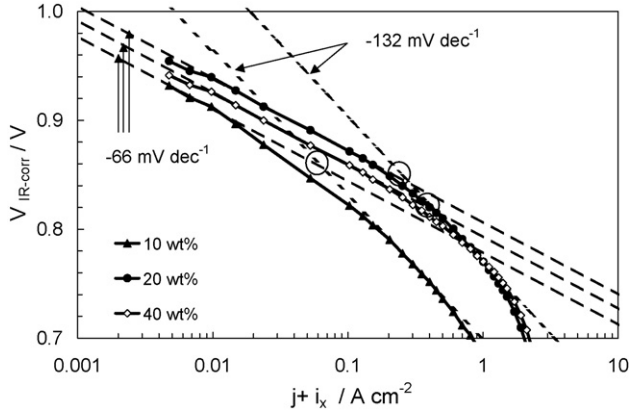

Fig. 3. Tafel plots of IR-corrected *V–j* curves measured with oxygen and hydrogen. The lines labelled $-66\,\text{mV}\,\text{dec}^{-1}$ are single Tafel slope approximations to the lcd part of the curve, the lines labelled $-132\,\text{mV}\,\text{dec}^{-1}$ are double Tafel slope approximations to the hcd part of the curves. The circles denote the intersection of the single and double Tafel slope approximations.

and

$$i_{\text{s}}\,\text{at}\,0.9\,V_{\text{IR-corr}} = \frac{j\,\text{at}\,V_{\text{IR-corr}} = 0.9\,\text{V}}{m_{\text{Pt}}\,\text{ECSA}} \quad (5)$$

so

$$i_{\text{m}} = i_{\text{s}} \times \text{ECSA} \quad (6)$$

The value of 0.9 V is selected because transport losses will be minimal at this voltage. The average values of the mass and specific activity (i_{m} and i_{s}) of the cathodes are listed in Table 3. For comparison with literature data they have been rescaled to 1 bar oxygen, assuming first order kinetics. The values for the mass activity obtained for Hispec 9100 electrodes are quite high, more than twice as high as for the E-TEK electrodes, due to the high ECSA values. A clear optimum for i_{m} as well as for i_{s} was found at 20 wt% Nafion. For i_{s} values independent of the Nafion content were expected, as all effects of varying utilisation are incorporated in the ECSA. Probably the different values mainly reflect the inaccuracies associated with obtaining activities from *V–j* curves. In the case of 10 wt% Nafion electrodes, transport limitations probably are already significant at 0.9 V. The other i_{s} values compare well to the E-TEK value, although lower values were expected due to the smaller particle size [22]. The specific activity data listed here are lower than reported recently by Gasteiger [1] for TKK and E-TEK catalysts. The data reported by Gasteiger were obtained at 80 °C. The difference between the average i_{s} of $140\,\mu\text{A}\,\text{cm}^{-2}$ at 65 °C and $200\,\mu\text{A}\,\text{cm}^{-2}$ at 80 °C corresponds to an activation energy of $28\,\text{kJ}\,\text{mol}^{-1}$, somewhat smaller than published values [23,24].

Another characteristic kinetic parameter is the Tafel slope *b*. It was also determined from the low current density part of the *V–j* curves measured with oxygen. The IR-corrected *V–j* curve at low current density is given by

$$V_{\text{IR-corr}}(j + i_x) = E^0(p_{\text{H}_2}, p_{\text{O}_2}) + b \log i_0 - b \log(j + i_x) \quad (7)$$

The kinetic Tafel slope could well be determined for the cathodes with ≥15 wt% Nafion from 5 to 6 points in the range of 10–100 $\text{mA}\,\text{cm}^{-2}$. The value obtained for *b* was $66\,\text{mV}\,\text{dec}^{-1}$ (Fig. 3). According to theory [25,26], the Tafel slope for the oxygen reduction reaction in the high potential region (0.8–1 V versus NHE), where the Pt is oxide-covered, is *RT*/*F*, i.e. $67\,\text{mV}\,\text{dec}^{-1}$ at 65 °C, in good agreement with the values obtained here. Fig. 3 shows that the single Tafel slope approximations to the curves fail beyond a certain current density. This due to transport losses as will be discussed below.

Table 3
Kinetic parameters for various electrodes at 65 °C (activities rescaled to 1 bar oxygen)

	Hispec 9100 56 wt% Pt AC01					E-TEK 40 wt% Pt Vulcan XC-72
Nafion wt%	10	15	20	30	40	30
i_m at 0.9 $V_{IR\text{-}corr}$ (A g^{-1} Pt)	52	89	111	82	79	48
i_s at 0.9 $V_{IR\text{-}corr}$ (μA cm^{-2} Pt)	79	139	165	153	126	143
b (mV dec^{-1})	66					68

3.5. Proton transport losses in V–j curves

At high current density proton resistance and mass transfer are no longer negligible. When saturated oxygen is used at the cathode, the oxygen concentration can, as a first approximation, be considered constant, i.e. oxygen transport losses are neglected. The voltage losses in an electrode where only kinetic and proton transport losses occur, are governed by Ohm's law describing proton transport

$$\frac{d\eta(z)}{dz} = R_p j_H(z) \text{ with } \eta(1) = \eta_1 \quad (8)$$

and an equation describing the generation of the current, e.g. the Tafel equation

$$\frac{dj_H(z)}{dz} = i_0 \exp\left(\frac{\eta}{b}\right) \text{ with } j_H(0) = 0 \quad (9)$$

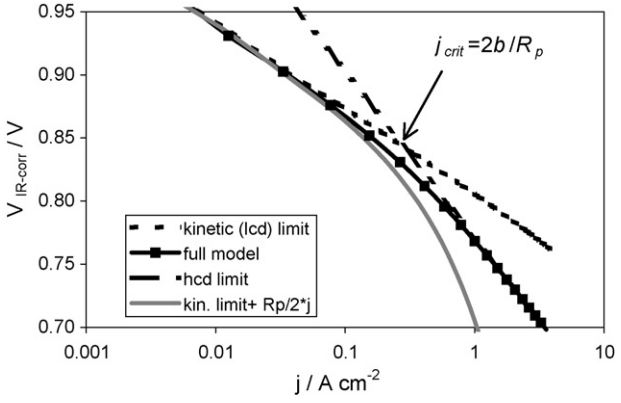

Fig. 4. Model curves incorporating kinetic effects and proton conduction losses in the electrode, calculated with $E^0 = 1.19$ V, $R_P = 0.2\ \Omega\ cm^2$, $b = 66$ mV dec^{-1} and $i_0 = 1.6\ 10^{-6}$ A cm^{-2}.

Here $j_H(z)$ is the proton current density in the electrode, R_P the proton resistance of the electrode and z the position in the cross section of the electrode (0 near the GDM, 1 near the membrane). The corresponding electronic current density is $j(z) = j - j_H(z)$, with j the total current density in the MEA. Notice, that the electronic resistance of the electrode is neglected. The Eqs. (8) and (9) can be solved analytically as well as numerically [27,28]. At very low current density (lcd) the solution converges to the limit given by Eq. (7), i.e. proton transport can be neglected entirely. At high current density (hcd) the solution has the limit

$$V_{IR\text{-}corr}(j + i_x) = E^0(p_{H_2}, p_{O_2}) + b \log i_0 + b \log\left(\frac{2b}{R_p}\right) - 2b \log(j + i_x) \quad (10)$$

This is the case of the so-called double Tafel slope. Fig. 4 shows an example of the full solution as well as both corresponding limiting solutions. The intersection of the limiting solution curves is at $j_{crit} = 2b/R_p$. The lcd solution is valid at current density $j \ll j_{crit}$, and the hcd solution at $j \gg j_{crit}$. Fig. 5 schematically shows the proton current density as a function of position in the electrode. In the lcd limit the proton current decreases steadily going from membrane ($z = 1$) to GDM, i.e. the reaction rate is the same at any position. In the hcd limit the reaction occurs mainly near the membrane/electrode interface. This is accompanied by a higher overpotential near the interface compared to an almost constant overpotential in the lcd limit. As long as the reaction rate is evenly distributed over the electrode, proton conduction losses can easily be obtained from the integration of Ohm's law resulting in $jR_p/2$ and the total equation for $V_{IR\text{-}corr}$ might be approximated by

$$V_{IR\text{-}corr}(j + i_x) = E^0(p_{H_2}, p_{O_2}) + b \log i_0 - b \log(j + i_x) + \frac{R_p}{2} j \quad (11)$$

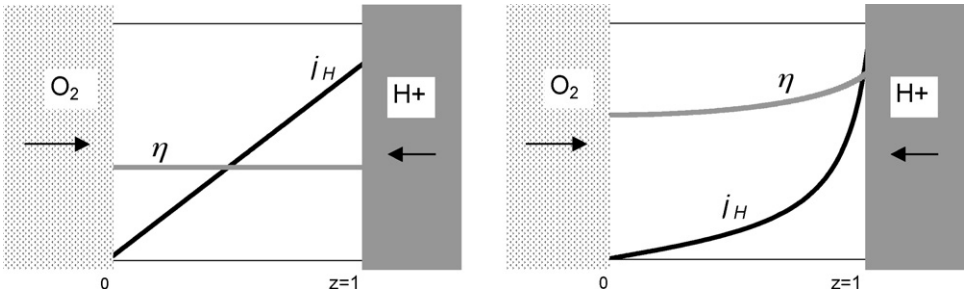

Fig. 5. Schematic representation of the proton current density and overpotential in the cross section of the cathode according to model calculations at low current density (left) and high current density conditions (right), respectively.

Fig. 4, however, shows that this approximation deviates already substantially from the full curve at current densities much smaller than j_{crit}. Use of Eq. (11) to obtain R_p from a V–j curve would result in seriously underestimated values.

As discussed in the previous section Fig. 3 shows the single Tafel slope approximation (Eq. (7) with $b = 66\,\text{mV dec}^{-1}$) to IR-corrected curves measured with oxygen. Also shown are double Tafel slope approximations calculated according to equation 10 ($2b = 132\,\text{mV dec}^{-1}$). The current density at the intersection of the single and double Tafel slope increases with increasing Nafion content. This means that as expected the R_p decreases with Nafion content. The critical current densities are between 0.1 and 0.5 A cm^{-2}, i.e. well in the operating range of the fuel cell. The estimated R_p values are between 0.6 and 0.1 Ω cm^2. The y-axis intercept of the double Tafel slope was optimised in a fit of selected points in the hcd regions. The selection of these points is somewhat arbitrary which makes this graphical method of obtaining R_p not very accurate.

Note, that the variation in voltage and current density of the intersection of single Tafel and double Tafel slope curves suggests that the transition is indeed due to proton transport limitation and not to kinetic effects. It is well known that also the kinetic Tafel slope can increase from RT/F to $2RT/F$ when the Pt surface changes from oxide covered to oxide-free [25,26]. For bulk Pt this transition takes place at 0.8 V versus NHE, for smaller particles it shifts to lower voltage [29,30].

3.6. Proton resistance from EIS measurements

A more reliable estimate of R_p can be obtained from EIS measurements with oxygen. With a similar model as used above, i.e. Tafel kinetics and proton resistance as limiting factors, it can be derived that at high frequency the impedance of the MEA can be written as [31–33]

$$Z_t^{hf}(\omega) = R_{hf} + \sqrt{\frac{R_p}{C_{dl}}}\omega^{-1/2}\frac{\sqrt{2}}{2}(1-i) \tag{12}$$

This means that at high frequency the Nyquist plot of the MEA, after correction for the ohmic resistance R_{hf}, displays a 45° line. When the modulus of the impedance in this region is plotted versus $\omega^{-1/2}$, a straight line results with slope $\sqrt{R_p/C_{dl}}$. R_p can now be calculated using the C_{dl} data obtained from cyclic voltammetry.

Nyquist plots obtained at $j = 50\,\text{mA cm}^{-2}$ for several Hispec 9100 MEAs are shown in Fig. 6. The arc shown is due to the charge transfer reaction, i.e. the kinetics of the oxygen reduction. The 45° region is visible, especially at low Nafion content. At very high Nafion content the R_p value is probably so low that the charge transfer arc dominates. The absolute values of impedances Z with phase angle $-40° < \phi < -50°$ were plotted versus $\omega^{-1/2}$. R_p values were obtained from the slope of these lines according to Eq. (12) using the capacitance values measured for that MEA in cyclic voltammetry studies. The values obtained are shown in Fig. 7, including those obtained at other values of the current density. The values show little variation with the current density except for the electrode with 10 wt% Nafion. In this case the proton resistance is high and decreases with current density probably due to changes in the water content of the ionomer phase. At 15, 20, 30 and 40 wt% the R_p values were 0.6, 0.19, 0.09 and 0.08 Ω cm^2, respectively, corresponding to critical current densities of 100, 315, 666 and 750 mA cm^{-2}.

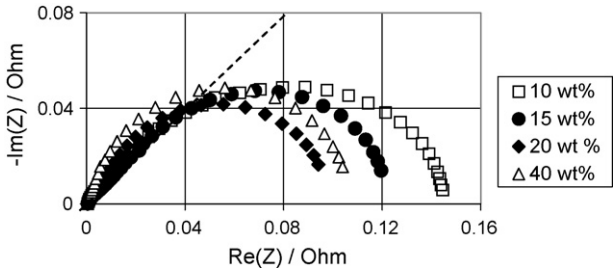

Fig. 6. Nyquist plot of the impedance at $j = 50\,\text{mA cm}^{-2}$ of electrodes with varying Nafion content under oxygen.

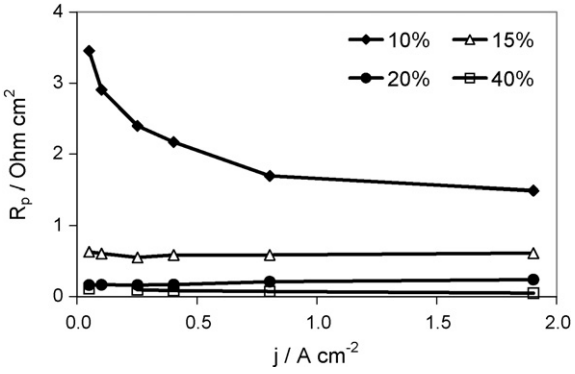

Fig. 7. Proton resistance determined from EIS as a function of current density for electrodes with varying Nafion content.

In Fig. 8 the R_p values from EIS at 400 mA cm^{-2} have been plotted as a function of the volume fraction of Nafion. The data obtained with 10 wt% Nafion have been omitted because of the large dependency on the current density. It is usually assumed that the proton resistance depends on the thickness L of the electrode and the Nafion volume fraction ε_{Nafion} according to [20,34]

$$R_p = \frac{L}{\sigma_{ion}\varepsilon_{Nafion}^{m}} \tag{13}$$

Here σ_{ion} is the effective bulk proton conductivity of the electrode. The volume fractions corresponding to each wt% Nafion

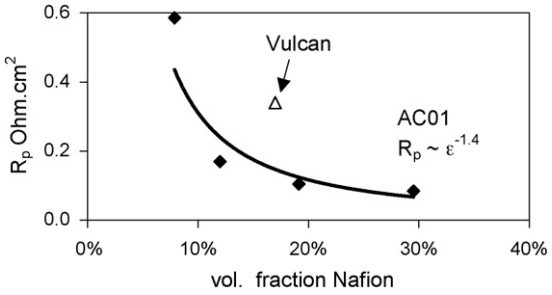

Fig. 8. Proton resistance of the electrode as a function of the Nafion volume fraction.

are listed in Table 1. Fig. 8 shows that R_p decreases with the Nafion volume fraction. The drawn line in Fig. 8 is a curve fitting the data with $m = 1.4$. This is quite close to the Bruggeman factor of 1.5 for transport in porous media. For the factor L/σ_{ion} a value of 0.012 Ω cm^2 was found. With $L = 8$ μm this corresponds to $\sigma_{ion} = 0.07$ S cm^{-1}. This is in the range of values found for bulk Nafion at this temperature [35]. A low value was expected since the Nafion layers covering the Pt/C will be very thin [2], in the order of a few nm. However, due to overlap of Nafion layers in pores of the electrode, the real layer thickness will at many locations be higher than the nominal thickness. The proton resistance of 11 μm thick electrodes based upon Vulcan was found to be 0.34 Ω cm^2 with 17 vol% Nafion. When accounting for the thickness this value is in fair agreement with data obtained here.

3.7. Performance with air: oxygen transport and oxygen gain

The oxygen gain, i.e. the difference in performance with oxygen and with air at the cathode, is shown in Fig. 9. The oxygen gain increases over the whole current density region. There is a contribution from the gas diffusion medium and a small contribution from kinetics but these should be similar for all Hispec 9100 electrodes considered [2]. The differences between the curves are related to the differences in transport losses in the electrode active layer. It is seen that the oxygen gain is smallest for the MEAs with 20 wt%. Nafion in the electrode. In the electrodes with more Nafion the pore volume is less and gas transport is limited. However, also in the electrodes with less than 20 wt% Nafion oxygen gain is higher than at 20 wt%.

Electrode models can help to understand this behaviour. There are two models available to describe the oxygen transport in porous electrodes, coupled to proton transport and electrode kinetics. The agglomerate model assumes the oxygen diffusion limitations are in the agglomerates of the electrode, with the agglomerate radius as the characteristic dimension [36,37]. In the pseudohomogeneous model it is assumed oxygen transport through the electrode thickness is limiting, with characteristic length L [27,28]. Both models have in common that beyond a certain current density j_{dif} oxygen transport limitations become severe. In the *absence* of proton transport limitations, i.e. $R_p = 0$ and infinite j_{crit}, both models predict $V_{IR\text{-}corr}(j)$ corrected curves

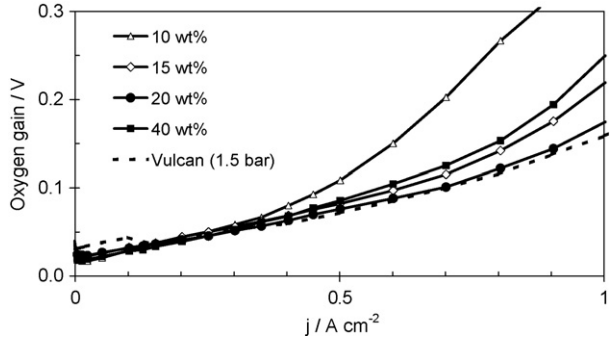

Fig. 9. The oxygen gain as a function of current density in MEAs with varying Nafion content in the electrodes.

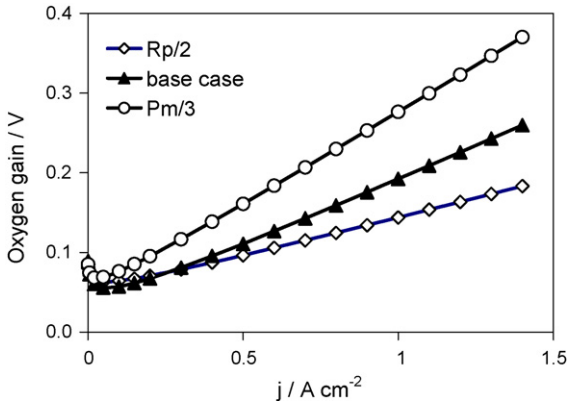

Fig. 10. Oxygen gain calculated using the pseudohomogeneous model. The base case performance with oxygen was calculated using the parameters listed in the caption of Fig. 4. For the base case performance with air the same parameters were used except $E^0 = 1.18$ V, an average oxygen fraction y of 0.15 and an oxygen permeability $P_m = 3 \times 10^{-9}$ mol s^{-1} cm^{-1} bar^{-1}. The figure shows the effect on the oxygen gain of the reduction of R_p by a factor of two, and of the reduction of the permeability P_m by a factor of 3.

with a double Tafel slope for $j \gg j_{dif}$. However, also according to both models, the transport losses increase dramatically, when j exceeds both j_{dif} and j_{crit}.

In the agglomerate model an analytical solution for the case $j \gg j_{crit}$ and $j \gg j_{dif}$ can be found [36,37]

$$V_{IR\text{-}corr}(j + i_x) = E^0(p_{H_2}, p_{O_2}) + b\log(i_0 y) + b\log(Xy) + 2b\ln\frac{2b}{R_p} - 4b\log(j + i_x) \quad (14)$$

Here X is a measure for the agglomerate diffusion and y for the oxygen pressure. Eq. (14) implies there is a second doubling of the Tafel slope. Subtraction of Eq. (10) from Eq. (14) results in the oxygen gain and it is clear that this increases directly with R_p, as well as with X. For the pseudohomogeneous model an analytical solution for this limit is not available. Results of numerical calculations of the oxygen gain are shown in Fig. 10. Again, the direct dependence of the oxygen gain on R_p as well as on the oxygen permeability P_m is clear. This is related to the phenomenon shown in Fig. 5. When air instead of pure oxygen is used, the finite oxygen transport limits the reaction near the interface thus decreasing the reaction rate near the interface and increasing it near the GDM, at the expense of larger proton transport losses. Notice, that the permeability parameters P_m and X can depend on the water content. Hence, they may change with current density. The volume in the electrode occupied by Nafion may increase due to swelling, at the expense of void volume. Therefore model calculations using fixed values may underestimate the oxygen gain at high current density.

The V–j characteristics measured with air are shown in Fig. 11. It is clear that the MEAs with 20 wt% Nafion in the cathode performed best at all current densities. In the MEAs with high Nafion content the oxygen diffusion is now limited by Nafion blocking the pores. At low Nafion content the high R_p limits the performance.

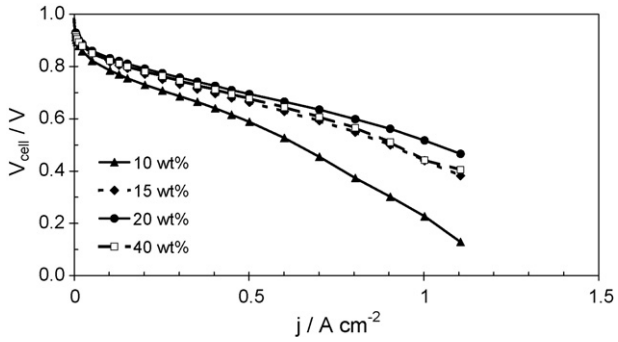

Fig. 11. Averaged *V–j* curves measured with hydrogen and air for MEAs with varying Nafion content.

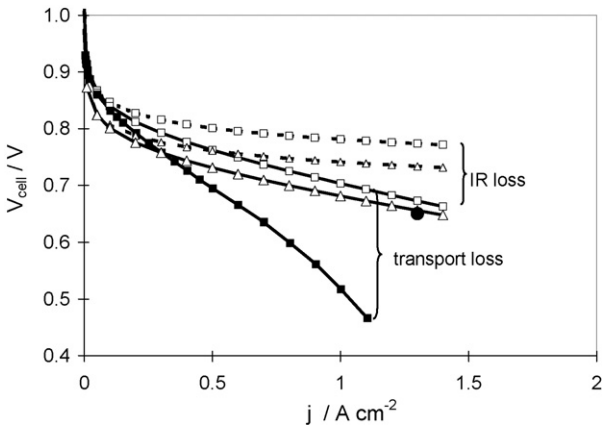

Fig. 12. Comparison of automotive target (represented by ●) to the measured (solid line, marker ■) performance. The dashed lines represent the IR-free performance of a cathode operating in the kinetic limit with 0.4 mg Pt cm^{-2} (□) and 0.1 mg Pt cm^{-2} (Δ) respectively. The solid lines with open markers represent curves without transport losses, calculated for 0.4 mg Pt cm^{-2} and $R_{hf} = 0.08\ \Omega\,cm^2$ (□), and 0.1 mg Pt cm^{-2} and $R_{hf} = 0.06\ \Omega\,cm^2$ (Δ), respectively.

4. Discussion

As a result of a high SA and a high utilisation the mass activity for the oxygen reduction reaction of the Hispec 9100 material was much higher than of the E-TEK material based upon Vulcan XC-72. Achieving high utilisation with high-surface-area carbon supports is not trivial, and in fact these two features seemed for some time to be at conflict [12,13]. Apparently in Hispec 9100 the Pt was dispersed on sites in pores well accessible to Nafion. Still, it seems that 40% of the Pt surface area could not be used for the oxygen reduction reaction, which suggests there is further room for improvement.

The specific activity of Pt on AC01 was not lower than of the E-TEK material in spite of the reduced particle size. This also contributed to the high mass activity. The Pt particles in Hispec 9100 are of the size (2.5–3 nm) that is considered optimal for a high mass activity, i.e. the size for which the product of the specific activity (increasing with size) and the SA (decreasing with size) is maximal [1].

The transport properties of the cathode were further characterised by analysis of the *V–j* characteristics and by EIS. The proton resistance of the electrode was found to play a crucial role for the performance with oxygen as well as air. Due to proton transport limitations the effective Tafel slope of the curves measured with oxygen doubles beyond a critical current density, j_{crit}, inversely proportional to the proton resistance. Also the oxygen gain, i.e. the voltage loss that is found at a given current density when air replaces oxygen, decreases with decreasing proton resistance. For a reduction of transport losses, the critical current density should be increased, ideally to values significantly exceeding the operational current density. With a kinetic slope of 65 mV dec^{-1} (i.e. 0.03 V) a j_{crit} of 1.5 A cm^{-2} would correspond to an R_p of 0.02 Ω cm^2. This can in part be achieved by a reduction of the thickness of the electrode, but also by modification of the ionomer phase.

For performance with air the optimal Nafion content was 20 wt% or a ionomer:carbon ratio of 0.6. This is also the value at which the oxygen gain was minimal and the utilisation optimal. It must be noted that, although the optimal weight percentage of Nafion in Hispec 9100 electrodes was lower than in 40 wt% Pt/Vulcan XC-72 electrodes (20 versus 30 wt%), the ionomer:carbon ratio was similar. The proton transport resistance in the Hispec 9100 based electrodes decreased with higher Nafion content but at the same time the permeability for oxygen was reduced. However, a different distribution of the Nafion over the electrode, e.g. by imposing a gradient of the Nafion content from GDM to membrane interface [38], may improve the proton conductivity while maintaining the other good properties.

A question addressed in the introduction of the paper was whether the new catalysts with high-surface-area carbon supports would be sufficiently good to meet the targets for automotive applications. With a Pt loading of 0.4 mg cm^{-2} at the cathode the current materials do not meet the required performance. Reduction of the Pt loading to 0.1 mg cm^{-2} would reduce the i_o in Eq. (7) by a factor of four, and hence introduce an additional kinetic voltage loss of $66 \times \log(4) = 40$ mV. This can in part be compensated by the use of a thinner membrane, i.e. 25 instead of 50 μm, reducing the ohmic resistance by 0.02 Ω cm^2. The oxygen gain at 1.4 A cm^{-2} would have to be reduced by 200 mV. Extrapolation of the data in Fig. 12 suggest that this corresponds to annihilation of all transport effects. Use of a lower Pt loading should reduce the thickness (from 8 to 2 μm) and hence the proton resistance and oxygen gain. So, the target may be achieved provided that structural improvements can be made that allow the electrode to operate in the kinetic limit up to 1.4 A cm^{-2}.

Even more demanding is the requirement that the electrode is stable, i.e. keeps up the performance at the required level. Pt particle growth and dissolution as well as carbon corrosion all result in increased cathode losses [39,40]. Carbon corrosion on these high-surface-area-carbons may well be higher than on Vulcan.

5. Conclusions

In this work it was found that thin-film cathodes based on high-surface-area carbon support catalyst material (56 wt% Pt/AC01 Hispec 9100 from Johnson Matthey) showed high ECSA values in the order of 65 m^2 g^{-1}. This is due to the high

specific surface area of the catalyst combined with a high utilisation of about 60%. As a result, the mass activity of platinum for the oxygen reduction in these electrodes was more than twice as high as found in thin film electrodes based on conventional 40 wt% Pt/Vulcan XC-72.

The optimum ionomer:carbon ratio for operation with air found for the electrodes based upon Hispec 9100 was 0.6. For this optimum content the proton resistance was lower than for the conventional electrodes, mainly due to the reduced thickness (25–30% thinner). A further reduction of this value is essential for the minimisation of all transport losses and might be achieved by further decrease of the electrode thickness and structure optimisation.

The activity of the Pt/AC01 (Hispec 9100) catalysts may just be sufficient for automotive applications providing the transport losses are minimized. Still, even then the stability of Pt particles as well as of the support is critical.

Acknowledgements

The authors wish to thank H.C.D. Smit (ECN) for MEA preparation, and C.M. Roos and C. van Egmond (ECN) for structural characterisation of powders and MEAs.

References

[1] H.A. Gasteiger, S.S. Kocha, B. Sompalli, F.T. Wagner, Appl. Catal. B: Environ. 56 (2005) 9–35.
[2] S.S. Kocha, in: W. Vielstich, H.A. Gasteiger, A. Lamm (Eds.), Handbook of Fuel Cells—Fundamentals, Technology and Applications, vol. 3, John Wiley and Sons, 2003, pp. 538–565.
[3] http://www.etek-inc.com/custom/index.php.
[4] http://www.3m.com/about3m/technologies/fuelcells/index.jhtml.
[5] http://www.gore.com/en_xx/products/electronic/fuelcells/series_56_mea_fuel_cells.html.
[6] http://www.tanaka.co.jp/products-e/products1/f_5.html.
[7] http://www.johnsonmattheyfuelcells.com/HiSPEC_Datasheet.pdf.
[8] H.A. Gasteiger, J.E. Panels, S.G. Yan, J. Power Sources 127 (2004) 162–171.
[9] M. Uchida, Y. Aoyama, N. Eda, A. Ohta, J. Electrochem. Soc. 142 (1995) 4143–4148.
[10] A. Lundblad, J. New Mater. Electrochem. Syst. 7 (2004) 21–28.
[11] http://www.johnsonmattheyfuelcells.com/HiSPEC_Customer_Chart.pdf.
[12] M. Uchida, Y. Fukoaka, Y. Sugawara, N. Eda, A. Ohta, J. Electrochem. Soc. 143 (1996) 2245–2252.
[13] V. Rao, P.A. Simonov, E.R. Savinova, G.V. Plaksin, S.V. Cherepanova, G.N. Kryokova, U. Stimming, J. Power Sources 1452 (2005) 178–187.
[14] E. Antolini, L. Giorgi, A. Pozio, E. Passalacqua, J. Power Sources 77 (1999) 136–142.
[15] E. Passalacqua, F. Lufrano, G. Squadrito, A. Patti, L. Giorgi, Electrochim. Acta 46 (2001) 799–805.
[16] J.M. Song, S.Y. Cha, W.M. Lee, J Power Sources 94 (2001) 78–84.
[17] G. Li, P.G. Pickup, J. Electrochem. Soc. 150 (2003) C745–C752.
[18] T.R. Ralph, M.P. Hogarth, Platinum Metals Rev. 46 (2002) 3–14.
[19] P. Gode, F. Jaouen, G. Lindbergh, A. Lundblad, G. Sundholm, Electrochim. Acta 48 (2003) 4175–4187.
[20] H.A. Gasteiger, W. Gu, R. Makharia, M.F. Mathias, B. Sompalli, in: W. Vielstich, H.A. Gasteiger, A. Lamm (Eds.), Handbook of Fuel Cells-Fundamentals, Technology and Applications, vol. 3, John Wiley and Sons, 2003, pp. 593–610.
[21] B.E. Easton, P.G. Pickup, Electrochem. Solid-State Lett. 3 (2000) 359–361.
[22] K. Kinoshita, Electrochemical Oxygen Technology, John Wiley & Sons, Inc., New York, 1992.
[23] P.D. Beattie, V.I. Basura, S. Holdcroft, J. Electroanal. Chem. 468 (1999) 180–192.
[24] H. Xu, Y. Song, H.R. Kunz, J.M. Fenton, J. Electrochem. Soc. 152 (2005) A1828–A1836.
[25] D.B. Sepa, M.V. Vojnovic, A. Damjanovic, Electrochim. Acta 26 (1981) 781–793.
[26] D.B. Sepa, M.V. Vojnovic, L. Vracar, A. Damjanovic, Electrochim. Acta 32 (1987) 129–134.
[27] T.E. Springer, M.S. Wilson, S. Gottesfeld, J. Electrochem. Soc. 140 (1993) 3513–3526.
[28] M. Eikerling, A.A. Kornyshev, J. Electroanal. Chem. 453 (1998) 89–106.
[29] N.M. Markovic, T.J. Schmidt, P.N. Ross, V. Stamenkovic, Fuel Cells 1 (2001) 105–116.
[30] S. Mukerjee, J. McBreen, J. Electroanal. Chem. 448 (1998) 163–171.
[31] R. DeLevie, Electrochim. Acta 8 (1963) 751–780.
[32] M. Eikerling, A.A. Kornyshev, J. Electroanal. Chem. 475 (1999) 107–123.
[33] R. Makharia, M.F. Mathias, D.R. Baker, J. Electrochem. Soc. 152 (2005) A970–A977.
[34] C. Boyer, S. Gamburzev, O. Velev, S. Srinivasan, A.J. Appleby, Electrochim. Acta 43 (1998) 3703–3709.
[35] T.A. Zawodzinski Jr., M. Neeman, L.O. Sillerud, S. Gottesfeld, J. Phys. Chem. 95 (1991) 6040–6044.
[36] M.L. Perry, J. Newman, E.J. Cairns, J. Electrochem. Soc. 145 (1998) 5–15.
[37] F. Jaouen, G. Lindbergh, G. Sundholm, J. Electrochem. Soc. 149 (2002) A437–A447.
[38] Z. Xie, T. Navessin, K. Shi, R. Chow, Q. Wang, D. Song, B. Andreaus, M. Eikerling, Z. Liu, S. Holdcroft, J. Electrochem. Soc. 152 (2005) A1171–A1179.
[39] P.J. Ferreira, G.J. la O', Y. Shao-Horn, D. Morgan, R. Makharia, S. Kocha, H.A. Gasteiger, J. Electrochem. Soc. 152 (2005) A2256–A2271.
[40] J. Xie, D.L. Wood, K.L. More, P. Atanassov, R.L. Borup, J. Electrochem. Soc. 152 (2005) A1011–A1020.